ISSN 1674-1056
http://cpb.iphy.ac.cn
http://iopscience.iop.org/cpb
中国物理 B
Chinese Physics
中国物理
Chinese Physics B

Composition effect on elastic properties of model NiCo-based superalloys

Weijie Li(李伟节), Chongyu Wang(王崇愚)
Citation: Chin. Phys. B . 2020, 29(2): 026102 . **doi:** 10.1088/1674-1056/ab6204
Journal homepage: http://cpb.iphy.ac.cn; http://iopscience.iop.org/cpb

What follows is a list of articles you may be interested in

Stability and mechanical properties of various Hf-H phases:A density-functional theory study

Wei Xiao(肖伟), Lu Sun(孙璐), Shu-Hui Huang(黄树晖), Jian-Wei Wang(王建伟), Lei Cheng(程磊), Li-Gen Wang(王立根)
Chin. Phys. B . 2017, 26(10): 106103 . **doi:** 10.1088/1674-1056/26/10/106103

Strain rate and cold rolling dependence of tensile strength and ductility in high nitrogen nickel-free austenitic stainless steel

Gui-Xun Sun(孙贵训), Yue Jiang(江月), Xiao-Ru Zhang(张晓茹), Shi-Cheng Sun(孙世成), Zhong-Hao Jiang(江忠浩), Wen-Quan Wang(王文权), Jian-She Lian(连建设)
Chin. Phys. B . 2017, 26(9): 096104 . **doi:** 10.1088/1674-1056/26/9/096104

Effects of pressure on structural, electronic, and mechanical properties of *α*, *β*, and *γ* uranium

Hui-Jie Zhang(张慧杰), Shi-Na Li(李世娜), Jing-Jing Zheng(郑晶晶), Wei-Dong Li(李卫东), Bao-Tian Wang(王保田)
Chin. Phys. B . 2017, 26(6): 066104 . **doi:** 10.1088/1674-1056/26/6/066104

Energetics of carbon and nitrogen impurities and their interactions with vacancy in vanadium

Juan Hua(华娟), Yue-Lin Liu(刘悦林), Heng-Shuai Li(李恒帅),Ming-Wen Zhao(赵明文), Xiang-Dong Liu(刘向东)
Chin. Phys. B . 2016, 25(3): 036104 . **doi:** 10.1088/1674-1056/25/3/036104

Effects of cold rolling deformation on microstructure, hardness, and creep behavior of high nitrogen austenitic stainless steel

Sun Shi-Cheng, Sun Gui-Xun, Jiang Zhong-Hao, Ji Chang-Tao, Liu Jia-An, Lian Jian-She
Chin. Phys. B . 2014, 23(2): 026104 . **doi:** 10.1088/1674-1056/23/2/026104

Composition effect on elastic properties of model NiCo-based superalloys*

Weijie Li(李伟节)[1,2] and Chongyu Wang(王崇愚)[1,†]

[1] *Department of Physics, Tsinghua University, Beijing* 100084, *China*
[2] *Institute of Applied Physics and Computational Mathematics, Beijing* 100088, *China*

(Received 7 June 2019; revised manuscript received 13 December 2019; accepted manuscript online 16 December 2019)

NiCo-based superalloys exhibit higher strength and creep resistance over conventional superalloys. Compositional effects on elastic properties of the γ and γ' phases in newly-developed NiCo-based superalloys were investigated by first-principles calculation combined with special quasi-random structures. The lattice constant, bulk modulus, and elastic constants vary linearly with the Co concentration in the NiCo solution. In the selected (Ni, Co)$_3$(Al, W) and (Ni, Co)$_3$(Al, Ti) model γ' phase, the lattice constant, and bulk modulus show a linear trend with alloying element concentrations. The addition of Co, Ti, and W can regulate lattice mismatch and increase the bulk modulus, simultaneously. W-addition shows excellent performance in strengthening the elastic properties in the γ' phase. Systems become unstable with higher W and Ni contents, *e.g.*, $(Ni_{0.75}Co_{0.25})_3(Al_{0.25}\ W_{0.75})$, and become brittle with higher W and Co addition, *e.g.*, $Co_3(Al_{0.25}\ W_{0.75})$. Furthermore, Co, Ti, and W can increase the elastic constants on the whole, and such high elastic constants always correspond to a high elastic modulus. The anisotropy index always corresponds to the nature of Young's modulus in a specific direction.

Keywords: NiCo-based superalloys, elastic constants, special quasi-random structures (SQS), directional Young's modulus

PACS: 61.82.Bg, 62.20.–x, 63.50.Gh, 71.15.Mb **DOI:** 10.1088/1674-1056/ab6204

1. Introduction

Hardness and ductility are two of the key parameters for the design and characterization of materials and these quantities largely depend on the elastic properties. New NiCo-based superalloys[1–4] show superior mechanical properties and creep properties: other researchers investigated the Ni–Co–Al–*X* quaternary systems and their distribution coefficients, using experimental investigation and thermodynamic modelling of Ni–Co–Al–W[5] and Ni–Al–Ti.[6] Experiments on Ni–Co–Al–W–Cr quinary model superalloys[5,7] have also been reported. An increase of Co-addition in Ni–Co–Al–W systems decreases the γ' solvus temperature and leads to a higher γ' volume fraction.[7] Ti-addition increases the anti-phase boundary energy of the γ' phase while reducing the alloy density,[8] but an excessive amount of Ti can form a $D0_{24}$ Ni_3Ti (η) phase. The disordered face-centred cubic (fcc) γ and $L1_2$ γ' phases formed with an fcc/$L1_2$ structure formed in the Ni–Al–Co–Ti quaternary alloy at 750 °C to 1100 °C in tests.[9] Atomic probe tomography shows that Co addition ($>$ 19%) decreases the solubility of Al and Ti in the γ' phase and caused Ni_3(Ti, Al) transformation in (Ni, Co)$_3$(Al, Ti) systems.[10] However, reports of concentration effect on mechanical properties of NiCo-based superalloys by first principles calculation remain sparse.

In the γ'-Co_3(Al, W) phase[11] of Co-based superalloys, Al and W randomly occupy the Al-sublattice. In NiCo-based superalloys, the precipitation of Ni and Co is complicated, they both randomly occupy sites in the γ phase and also exist in caused γ' phases. The first problem when studying NiCo-based superalloys is how to deal with the random problem caused by first principles calculation: the presence of a configurational substitutional disorder leads to a loss of translational periodicity. The prediction of the elastic properties of low-symmetry systems, such as random alloys, is less straightforward.

The widely used techniques for modelling disordered alloys are special quasi-random structures (SQS),[12] coherent potential approximation (CPA),[13] cluster expansion (CE),[14] and virtual crystal approximation (VCA).[15] The random distribution of impurity atoms in the CPA is elucidated in the framework of the mean-field approximation and ignore local lattice relations. The CE is based on the assumption that the energy (of any other scalar property) of the system can be expanded in terms of a set of well-chosen structural motives (figures) and the expansion parameters are typically obtained by fitting the CE Hamiltonian from *ab initio* electronic structure calculations. In the SQS, the randomness is introduced by mimicking as closely as possible the correlation functions of an infinite random alloy within a finite supercell. The calculation of electronic structure in SQS also involves local relaxation effects.

Here, we use first-principles calculation combined with

*Project supported by the National Key Research and Development Program of China (Grant No. 2017YFB0701502).
†Corresponding author. E-mail: cywang@mail.tsinghua.edu.cn
© 2020 Chinese Physical Society and IOP Publishing Ltd

SQS to investigate the strengthening mechanisms related to alloying elements and concentration on the elastic properties of NiCo-based superalloys, including the γ -NiCo phase and γ'-(Ni, Co)$_3$(Al, W/Ti) phase. The paper is organised as follows: Section 2 contains an introduction to the methods used, including SQS, the calculation of elastic constants using a strain-energy method, and elastic moduli derived from the elastic constants. Section 3 covers detailed information related to the calculations. Section 4 covers the result of first principles calculations, including lattice constant, bulk modulus, and elastic constants for all such the selected systems. Section 5 contains a discussion of the relationship between the lattice constant and bulk properties, and an analysis including stability, ductility, and electronic structure effects, *inter alia*, followed by salient conclusions.

2. Methods

2.1. SQS

Special quasi-random structure SQS[12,16] is a "special" N-atom periodic quasi-random structure S whose correlation function $\overline{\Pi}_{k,m}(S)$ best matches the ensemble averages $\left\langle \overline{\Pi}_{k,m}(S) \right\rangle_R$ of disorder systems. The degree of short-range order (SRO) is usually measured by the Warren–Cowley parameter α.[17] For binary $A_{1-x}B_x$ alloy and pseudo-binary $A_{1-x}B_xN$ alloy, it is defined as $\alpha = 1 - P_B(R)/x_B$, where $P_B(R)$ is the probability of finding a B atom at distance R from an A atom and x_B denotes the concentration of B. A perfectly random alloy is characterized by a vanishing α, while $\alpha > 0$ and $\alpha < 0$ correspond clustering and ordering, respectively.

$$\langle P \rangle = \sum_{\sigma} P(\sigma)\rho(\sigma), \tag{1}$$

$$\langle P \rangle = \sum_{f} p_f D_f \left\langle \overline{\Pi}_f \right\rangle, \tag{2}$$

where the configurational averages $\langle P \rangle$ can be accessed by identifying the leading terms in Eq. (2) and then constructing a single special configuration σ_s whose $\left\langle \overline{\Pi}_f(\sigma_s) \right\rangle$ is important. Then $P(\sigma_s)$ can be calculated for the single, special configuration σ_s without using any cluster expansion. $\langle P \rangle$ is thus approximated by $P(\sigma_s)$. For the random binary alloy $A_{1-x}B_x$ the correlation functions $\left\langle \overline{\Pi}_f \right\rangle$ are known trivially, *i.e.*, $\left\langle \overline{\Pi}_f \right\rangle = (2 \times -1)^{k_f}$, where k_f is the number of vertices in figure f. The basic advantage of this approach lies in its ability to describe disordered alloys with terms equivalent to those with which state-of-the-art methods address simple periodic crystals.

2.2. Elastic constants

The elastic constants can be calculated from the stress–strain, or strain–energy, methods. Since the total energy depends on the volume much more strongly than that on the strain,[18] we calculated elastic constants from the energy expansion using volume conserving deformations, *i.e.*, monoclinic (C_{44}) and orthorhombic distortions (C_{11}–C_{12}).

$$B = (C_{11} + 2C_{12})/3, \tag{3}$$

$$D_{\text{mono}} = \begin{pmatrix} 1 & \delta_m & 0 \\ \delta_m & 1 & 0 \\ 0 & 0 & 1/(1-\delta_m^2) \end{pmatrix},$$

$$\Delta E(\delta) = 2VC_{44}\delta^2 + O(\delta^4), \tag{4}$$

$$D_{\text{ortho}} = \begin{pmatrix} 1+\delta_o & 0 & 0 \\ 0 & 1-\delta_o & 0 \\ 0 & 0 & 1/(1-\delta_o^2) \end{pmatrix},$$

$$\Delta E(\delta) = V(C_{11} - C_{12})\delta^2 + O(\delta^4). \tag{5}$$

Considering the symmetry breaking, three crystallographic directions [001], [010], and [100] become inequivalent. We applied a symmetry-based projection technique[19,20] to predict the cubic elastic tensor of NiCo-based superalloys with the SQS approach.

The 21 inequivalent elastic constants of a triclinic system can be given as a vector with 21 components. In general, projector P^{sym} gives the closest elastic tensor with higher point group symmetry X^{sym} as

$$X^{\text{sym}} = P^{\text{sym}} X. \tag{6}$$

Then the closest cubic elastic tensor is given by

$$X^{\text{cub}} = \left(\overline{C}_{11}, \overline{C}_{11}, \overline{C}_{11}, \sqrt{2}\overline{C}_{12}, \sqrt{2}\overline{C}_{12}, \sqrt{2}\overline{C}_{12}, 2\overline{C}_{44}, 2\overline{C}_{44}, 2\overline{C}_{44}, 0,0,0,0,0,0,0,0,0,0,0,0\right), \tag{7}$$

where the projected cubic elastic constants $\overline{C}_{11}$, $\overline{C}_{12}$, and $\overline{C}_{44}$ are calculated by simple averaging, an approach used by von Pezold,[21]

$$\overline{C}_{11} = \frac{C_{11} + C_{22} + C_{33}}{3},$$

$$\overline{C}_{12} = \frac{C_{12} + C_{13} + C_{23}}{3},$$

$$\overline{C}_{44} = \frac{C_{44} + C_{55} + C_{66}}{3}. \tag{8}$$

We may also call them cubic-averaged elastic constants, as equation (8) is equivalent to averaging over the three crystallographic directions [100], [010], and [001]. According to this, nine independent tensor elements C_{11}, C_{22}, C_{33}, C_{12}, C_{13}, C_{23}, C_{44}, C_{55}, and C_{66} are needed to obtain the closest cubic projection of an elastic tensor with arbitrary symmetry. In the

following article, the averaged elastic constants $\overline{C}_{11}$, $\overline{C}_{12}$, and $\overline{C}_{44}$ are simply expressed as C_{11}, C_{12}, and C_{44}.

2.3. Elastic moduli

A series of elastic properties can be calculated by the elastic constants, *i.e.*, directional Young's modulus, shear modulus in a specific direction, and the elastic modulus of the polycrystalline materials.

2.3.1. Directional Young's modulus

The Young's modulus is the ratio of uniaxial stress to stain measured along the same axis and can be expressed as[22,23]

$$E_{[hkl]} = (S_{11} - (2S_{11} - 2S_{12} - S_{44})J)^{-1},$$
$$J = \frac{(h^2k^2 + k^2l^2 + h^2l^2)}{(h^2 + k^2 + l^2)^2}, \tag{9}$$

where subscripts h, k, and l represent the direction indices, $\boldsymbol{C}$ is the elastic constant tensor, $\boldsymbol{S}$ is the elastic compliance tensor, and $\boldsymbol{CS} = \boldsymbol{I}$. S_{ij} is a component of elastic compliance tensor $\boldsymbol{S}$. If $2S_{11} - 2S_{12} - S_{44} > 0$, the Young's modulus is maximised in the [111] direction and minimised in the [100] direction.

2.3.2. Shear modulus

The shear modulus G along [110] and [11$\bar{2}$] in the (111) plane can be determined by the calculated elastic constants.[24–26] The formulation for G is as follows:

$$G_{[110]} = \frac{3C_{44}(C_{11} - C_{12})}{2(C_{44} + C_{11} - C_{12})}, \tag{10}$$
$$G_{[11\bar{2}]} = \frac{3C_{44}(C_{11} - C_{12})}{4C_{44} + C_{11} + C_{12}}. \tag{11}$$

From its physical meaning, G along a specific direction corresponds to the slope of the stress–strain curve within the small strain limit. Without considering the phase transformation, crystal slip, formation of stacking faults, or other factors, G along a specific direction reflects the ideal shear strength along this direction to a certain extent. Furthermore, the Young's modulus in a specific direction reflects the ideal tensile strength along this direction to a certain extent.

2.3.3. Polycrystalline elastic modulus

For a polycrystalline aggregate, the principal crystallographic axes are mostly randomly oriented in space and the material is statistically isotropic. The bulk modulus B, shear modulus G, and anisotropy index A_Z are determined from elastic constants by Voigt–Reuss–Hill approximation.[22,27–29]

$$B_H = B_V = B_R = \frac{C_{11} + 2C_{12}}{3}, \tag{12}$$
$$G_V = \frac{C_{11} - C_{12} + 3C_{44}}{5},$$
$$G_R = \frac{5}{4S_{11} - 4S_{12} + 3S_{44}} = \frac{5C_{44}(C_{11} - C_{12})}{4C_{44} + 3(C_{11} - C_{12})},$$
$$G_H = \frac{1}{2}(G_V + G_R), \tag{13}$$
$$A_Z = \frac{2C_{44}}{C_{11} - C_{12}}, \tag{14}$$

where subscripts V, R, and H denote that the equations are derived from Voigt,[27] Reuss,[28] and Hill approaches,[29] respectively. A_Z gives the anisotropic variation of the sound velocity and of the angle between the displacement vector $\boldsymbol{u}$ and the wave vector $\boldsymbol{q}$ of the sound wave. The Pugh's approximation[30] can be adopted to characterise the material properties, *i.e.*, $B/G > 1.75$ implies ductile behavior, and $B/G < 1.75$ implies brittle behavior.

3. Calculations

3.1. SQS generation

Here, we selected the possible systems in NiCo-based superalloys, including: (i) NiCo solution (γ phase) both in the paramagnetic state and ferromagnetic state; (ii) binary $L1_2$ systems (γ' phase), including Co_3Al, Ni_3Al, Co_3 W, Ni_3 W, Co_3Ti, and Ni_3Ti; (iii) ternary $L1_2$ systems (γ' phase), including (Ni, Co)$_3$Al, Co$_3$(Al, W), Ni$_3$(Al, W), Co$_3$(Al, Ti), and Ni$_3$(Al, Ti); and (iv) quaternary $L1_2$ systems (γ' phase), including (Ni, Co)$_3$(Al, W), and (Ni, Co)$_3$(Al, Ti).

In a real alloy, the γ phase is an fcc random solution with Ni and Co occupying sites randomly when the Co concentration is below 65%. The shape of the (i) system supercell is $2[001] \times 2[010] \times 2[100]$, including 32 atoms as shown in Fig. 1(a). The Co concentration scale is 0%$\sim$ 62.5% with a step size of 12.5%. For the selected (ii) systems, a 64-atom lattice is constructed for the calculation of elastic constants. For the selected (iii) and (iv) systems with an $L1_2$ structure (Ni_3Al, Ni-sub-lattice, and Al-sub-lattice), Ni and Co atoms randomly occupy the Ni-sub-lattice while Al and W/Ti atom randomly occupy the Al-sub-lattice. The shapes of the supercells of (iii) and (iv) systems are $2[001] \times 4[010] \times 2[100]$, as shown in Fig. 1(b). In the 64-atom SQSs, 48 atoms comprise the Ni-sub-lattice and 16 comprise the Al-sub-lattice. The concentration scale in each type of site is 0%$\sim$ 100% with a step size of 12.5%.

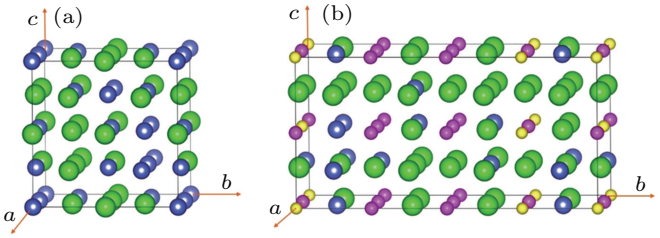


Fig. 1. SQSs in this calculation: (a) 32 atoms SQS for $Ni_{0.5}Co_{0.5}$ system, and (b) 64 atoms SQS for $(Ni_{0.75}Co_{0.25})_3(Al_{0.75}W_{0.25})$ system. The green balls represent Ni atoms, the blue balls represent Co atoms, the pink balls represent Al atoms, and the yellow balls represent W atoms.

The MedeA software give access to the 32-atom SQS in the whole concentration for the calculation of (i) systems (Fig. 1(a)). By employing the ATAT package,[31–33] the SQSs

were generated with shape restrictions over the entire concentration range for $L1_2$ cells containing 64 atoms of (iii), and (iv) systems. We generated SQSs using the following set of figures: all two-body clusters with edge length up to the ninth coordination shell, all three-body figures with edge length up to the fifth shell, all four-body figures with edge length up to the fourth shell, and all five-body figures with edge length up to the second shell.

3.2. VASP

After relaxation of the SQSs, the equilibrium lattice constants (a) and bulk modulus (B) were obtained by calculating the energy–volume dependence of the system and fitting it to the Murnaghan equation of state.[34] In the calculations of the elastic constants with cubic symmetry, a strain–energy approach is applied. Six types of deformations were adopted in the calculation of the elastic constants.

To obtain the total energies and extract the elastic constants of the supercells, density functional theory (DFT) calculations are conducted[35] by using the Vienna *Ab initio* Simulation Package (VASP),[36,37] a projector augmented wave method,[38] and the generalized gradient approximation (GGA)[39] in the parameterization introduced by Perdew, Burke, and Ernzerhop (PBE). The minimum cut-off of the plane wave energy is 350 eV. The spacing between k-points is 0.18 Å^{-1}. The spin-polarized calculation is considered in NiCo solution, in which the initial magnetic moment of Ni and Co are 0.65 μ_B and 1.6 μ_B, respectively.

4. Results

The calculated results are in good agreement with previous reported results (see Table 1). It should be pointed out that the type and concentration of the elements have an effective effect on the elastic properties of the systems. Furthermore, the calculation and experiment methods may also affect the results. So, some of our calculation results may have a little difference with the early reported experiment and calculation results.

Table 1. The equilibrium lattice constant (a, in unit Å), bulk modulus (B, in unit GPa), and elastic constants (C_{ij}, in unit GPa) of Ni, Ni_3Al, Co_3Al, Co_3W, and $Co_3(Al_{0.5}W_{0.5})$.

System	a/Å	B/GPa	C_{11}/GPa	C_{12}/GPa	C_{44}/GPa
Ni (PM)	3.516	195.2	248.9	168.4	111.2
experiments[a]	3.52	–	261.2	150.8	131.7
Ni_3Al	3.57	178.8	229.1	153.6	126.7
Calculations[b]	3.579	–	243.8	148.7	123.4
Experiments[c]	3.57[d]	174.9	227	148	120
$Co_3(Al_{0.5}W_{0.5})$	3.564	236.3	331.8	188.6	180.8
Calculations[e]	3.571	247.7	363.4	189.9	211.6
Calculations[f]	3.582	–	264	162	153
Experiments[g]	–	205	271	172	162

[a] Ref. [40], [b]Ref. [41], [c]Ref. [42], [d]Ref. [43], [e]Ref. [44], [f]Ref. [45], [g]Ref. [46].

4.1. Lattice constant and bulk modulus

From Fig. 2, the lattice constants and bulk moduli of the selected systems are linear functions of the alloy composition, which implies that the systems obey Vegard's law.[47] One has relationships such as $a_\gamma = a^0_\gamma + \sum_i \Gamma_i^\gamma x_i^\gamma$ and $a_{\gamma'} = a^0_{\gamma'} + \sum_i \Gamma_i^{\gamma'} x_i^{\gamma'}$ so that the lattice constants are linear with the mole fractions of added solutes. The Vegard coefficients Γ_i^γ and $\Gamma_i^{\gamma'}$ exhibit a strong dependence on the position of i in the periodic table. For simplicity, the rule of mixture[27–29] representing a weighted mean of the parameters of pure constituents is applied:

$$M^{\mathrm{p}} = \sum_i^N c_i M_i, \quad \sum_i^N c_i = 1, \tag{15}$$

where c_i denotes the concentration of component i in the alloy and M_i is the physical parameter of pure metal i in an fcc structure. For the NiCo systems, the values of c_i are listed in Table 2. It is clear that Co plays an important role in strengthening the γ phase.

From the definition of the lattice mismatch δ, we obtain,

$$\delta = 2\frac{a_{\gamma'} - a_\gamma}{a_{\gamma'} + a_\gamma} \times 100\%. \tag{16}$$

Usually, the lattice mismatch of Ni-based superalloys is negative, *i.e.*, $0.1\% < |\delta| < 0.5\%$,[48] while the lattice mismatch of Co-based superalloys is positive, *i.e.*, larger than 0.5%. The addition of Co leads to the reduction of the lattice constants in the selected systems, as shown in Figs. 2(a), 2(c), and 2(e), across the whole concentration scale. The addition of W and Ti into the Al-sub-lattice of γ' phases increases the lattice constants. For NiCo solution in a paramagnetic state, the addition of Co introduces −0.060-Å changes in the lattice constants per unit concentration change. In Ni_3Al, the addition of Co instead of Ni-sub-lattice introduces −0.031-Å changes in the lattice constants per unit concentration change and, the addition of W instead of Al-sub-lattice introduces +0.081-Å changes in the lattice constants per unit concentration change, the addition of Ti instead of Al-sub-lattice introduces +0.046-Å changes in the lattice constants per unit concentration change. Atom probe tomography experiments on NiCo-based superalloys show that, Co is preferentially distributed into the γ phase while Ti is preferentially distributed into the γ' phase.[10] From the perspective of regulating lattice mismatch, the addition of Co can decrease the lattice constant of the γ phase while the addition of Ti and W increases the lattice constant of γ' phase, which thus leads to a lattice mismatch of NiCo-based superalloys as they change from negative to positive.

The addition of Co, Ti, and W all causes to an increase in bulk modulus (Fig. 2): for NiCo solution in a paramagnetic state, the addition of Co introduces +52.21-GPa change in bulk modulus per unit concentration. In Ni_3Al, the addition

of Co instead of Ni-sub-lattice introduces +28.55-GPa change in bulk modulus per unit concentration, the addition of W instead of Al-sub-lattice introduces +52.48-GPa change in bulk modulus per unit concentration, the addition of Ti instead of Al-sub-lattice introduces +6.50-GPa change in bulk modulus per unit concentration. The Co, Ti, and W all show a strengthening effect on the bulk modulus. The presence of Co element in NiCo-based superalloys results in regulation of the lattice mismatch and improvements in the mechanical properties. W can strengthen the bulk modulus but also cause expansion of the γ' phase, and the Ti effect is weaker than that of W.

Table 2. Linear coefficients of NiCo solution in paramagnetic (PM) and ferromagnetic (FM) states, considering pure Ni as the benchmark.

	NiCo (PM)		NiCo (FM)	
	Intercept	Slope	Intercept	Slope
a/Å	3.517	−0.060	3.523	−0.002
B/GPa	195.33	52.21	192.25	14.39
C_{11}/GPa	241.90	146.30	268.66	19.17
C_{12}/GPa	172.05	5.14	154.04	12.02
C_{44}/GPa	105.87	89.78	134.40	16.83

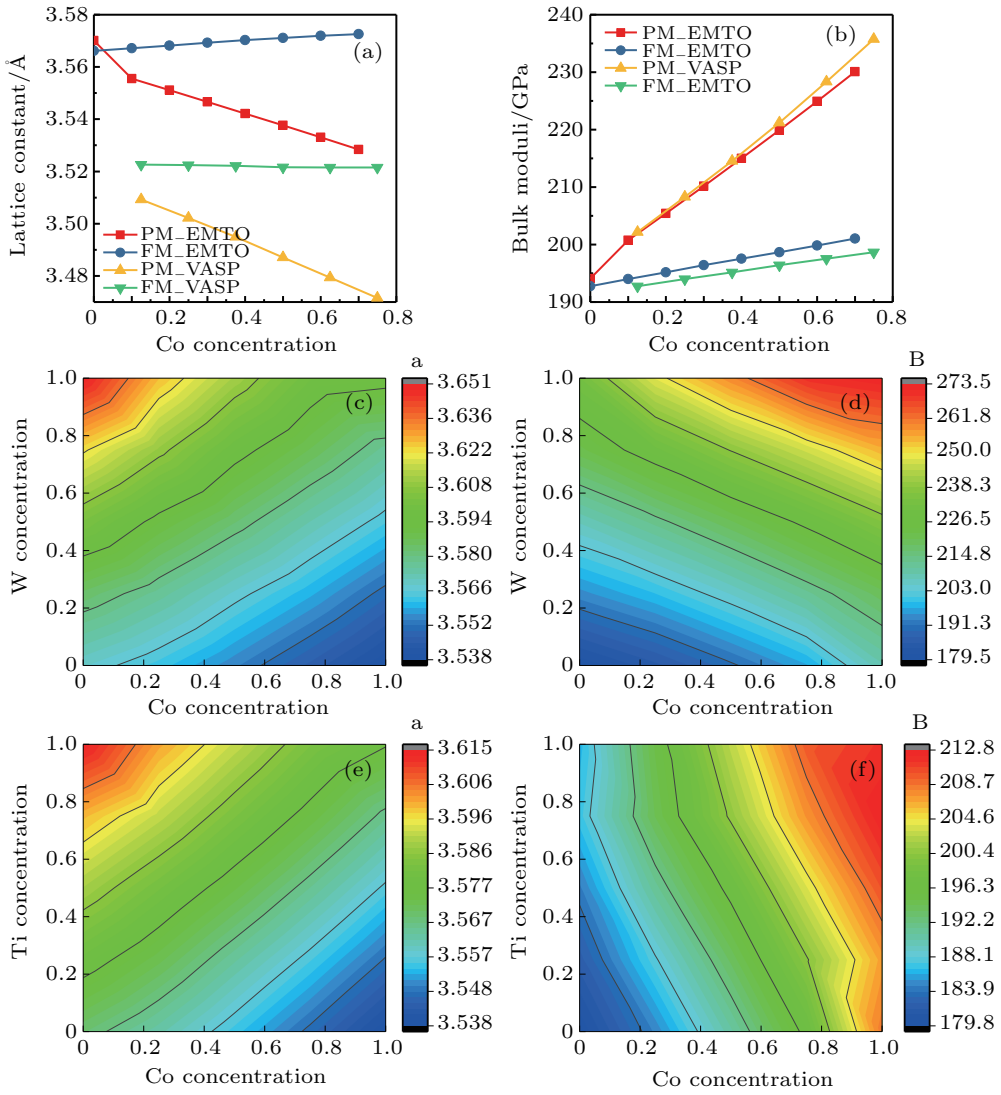


Fig. 2. Calculated lattice constant (in unit Å) and bulk modulus (in unit GPa) in NiCo solution, (Ni, Co)$_3$(Al, Ti), and (Ni, Co)$_3$(Al, W) systems: [(a), (c), and (e)] lattice constants in NiCo solution, (Ni, Co)$_3$(Al, W) and (Ni, Co)$_3$(Al, Ti); [(b), (d), and (f)] lattice constants in NiCo solution, (Ni, Co)$_3$(Al, W), and (Ni, Co)$_3$(Al, Ti).

4.2. Elastic constants

In Fig. 3(a), for NiCo solution in paramagnetic state, the addition of Co introduces +146.3-GPa change in C_{11} per unit concentration, +89.78-GPa change in C_{44} per unit concentration, and only +5.14-GPa change in C_{44} per unit concentration. The elastic constants of NiCo solution in ferromagnetic state change little, and no further discussion is needed. The relationship between elastic constants and Co concentration is quasi-linear (Table 2). In Fig. 3(b), C_{44} and C_{11} of (Ni, Co)$_3$X systems increase with Co addition, but C_{12} for (Ni, Co)$_3$W systems decreases with Co addition. The value of C_{44} of (Ni, Co)$_3$W is lower than that for Ni$_3$Al. In Fig. 3(b), the elastic constants of X_3(Al, W) increase with W addition, except for C_{44} of Ni$_3$(Al, W). The value of C_{11} of X_3(Al, Ti) increases with Ti addition, but C_{12} of Ni$_3$(Al, Ti) is lower than that of Ni$_3$Al. In Fig. 3(d), the elastic constants of the quaternary sys-

tem are higher than those of Ni_3Al (124.36 GPa), except for C_{44} (119.62 GPa) of $(Ni_{0.75}Co_{0.25})_3(Al_{0.25}W_{0.75})$. The elastic constants of the quaternary systems increase upon Co addition. The elastic constants of the Ni–Co–Al–W systems generally increase upon W addition. On the whole, the strengthening effect of W is higher than that of Ti on the elastic constants. In terms of the elastic constants, Co addition can strengthen C_{11} and C_{12} of both the γ and γ' phases.

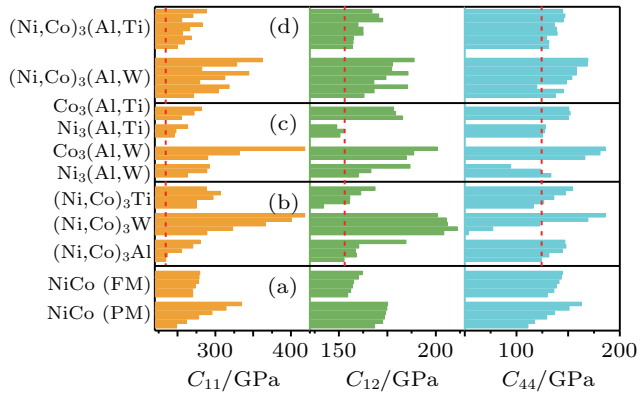


Fig. 3. Elastic constants C_{11}, C_{12}, and C_{44} for the selected systems. The systems are classified into four categories: (a) NiCo solutions including paramagnetic (PM) and ferromagnetic (FM) states, (b) (Ni, Co)$_3X$ including (Ni, Co)$_3$Al, (Ni, Co)$_3$W, (Ni, Co)$_3$Ti and all binary systems, (c) other ternary systems including W or Ti elements, and (d) quaternary systems. The vertical ordinate in this figure (Co, W, and Ti concentrations) increases in each system, and in panel (d) the W/Ti concentration changes first and then the Co concentration changes.

5. Discussion

5.1. Relationship between bulk modulus and volume

The bulk modulus of free-electron-like metals varies significantly with the atomic volume V when different elements are compared, and V does not depend much on the lattice structure as long as the electronic structure is not much changed.[22] We tested the relationship utilizing the bond valence based on the uniform electron gas model for transition metals.[49] Based on a published calculation method[41] and electron density results,[50] figure 4 illustrates the changes in bulk modulus with respect to electron density and volume.

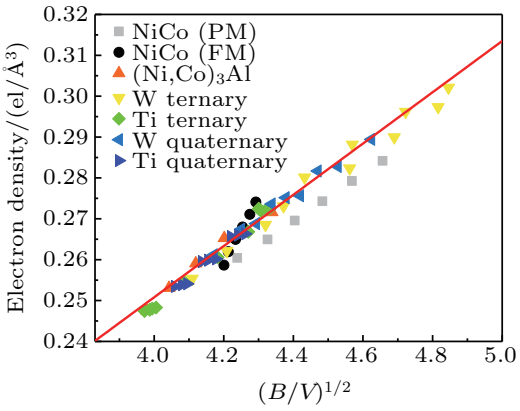


Fig. 4. Linear relationship between electron density and $(B/V)^{1/2}$ of Ni_3Al-type alloys. The red line fits data from systems with $L1_2$ structures, with a slope of 0.0627.

5.2. Stability and ductility

Before providing further analysis of the elastic properties, we analyze their stability and ductility.

5.2.1. Stability

In the Ni–Co binary phase diagrams, the NiCo solution is an fcc structure with a Co concentration below 65%. In the binary systems, the stable structure of Ni_3Al and Co_3Ti is $L1_2$, the stable structure of Co_3W is $D0_{19}$, the stable structure of Ni_3Ti is $D0_{24}$, and $L1_2$ is not a stable structure for Co_3Al. In the Ni–W binary phase diagrams, there are stable intermetallic compounds of Ni_4W and Ni_2W present, and the stable structure of Ni_3W is $D0_{22}$.[51] Here, we provide a stability analysis of ternary and quaternary systems with $L1_2$ crystal structures, and do not do so for NiCo solution and binary systems. Three methods were adopted to measure the structural stability, *i.e.*, the Born stability criteria,[52] formation energy, and pseudo-gap.

The Born stability criteria for cubic crystals are

$$C_{11} > |C_{12}|, \quad C_{44} > 0, \quad C_{11} + 2C_{12} > 0. \tag{17}$$

All the results in this study are within the limit of mechanical stability, satisfying the Born stability criteria.

The formation energy of the alloy was calculated using the constituent pure elements as reference states as follows:

$$\begin{aligned} &\Delta H((Ni_x, Co_{1-x})_3(Al_y, M_{1-y})) \\ &= E((Ni_x, Co_{1-x})_3(Al_y, M_{1-y})) - 0.75xE(Ni) \\ &\quad - 0.75(1-x)E(Co) - 0.25yE(Al) - 0.25(1-y)E(M), \end{aligned} \tag{18}$$

where E(Ni), E(Co), E(Al), and E(M) are the first-principles calculated total energies (per atom) of the constituent pure elements Ni, Co, Al, and M at the most stable states, *i.e.*, Ni and Al are fcc, Co and Ti are hexagonal close-packed (hcp), and W is body-centred cubic (bcc). All the formation energy in the Ni–Co–Al–Ti system is negative, which means that all the possible concentration combinations can form stable structures. With more Ti occupying the Al sites, they become more stable, as reported elsewhere.[53] In the Ni–Co–Al–W system, the formation energy of several structures is positive when the W concentration is high, such as, $(Ni_{0.75}Co_{0.25})_3W$. The position of the pseudo-gap shows that $(Ni_{0.75}Co_{0.25})_3(Al_{0.25}W_{0.75})$ is unstable. The systems tend to be unstable at higher Ni and W.

5.2.2. Ductility

Here, Pugh's approximation[30] and the Cauchy pressure are adopted to evaluate the mechanical properties of the selected systems with various alloying concentrations,[54,55] as shown in Fig. 5. The Pugh's modulus ratio G/B reflects the competition between the shear and cohesive strength at the crack tip of fracture, and the brittle-ductile limit is suggested to

be around $B/G = 1.75$. On the other hand, a negative Cauchy pressure is suggested as being associated with covalent interatomic bonding.[56] An understanding of Cauchy pressure is related to an understanding of crystal structure trends in the transition metals. In Fig. 5, the higher Co or W of the γ' phase tends to become brittle.

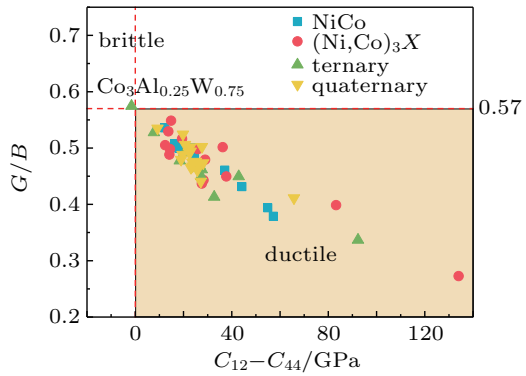


Fig. 5. The G/B *versus* Cauchy pressure maps of the systems (the legend corresponds to the systems shown in Fig. 3).

5.3. Elastic modulus

From the elastic constants results of Subsection 4.2, we provide an analysis of the shear modulus along the main shear direction, and directional Young's modulus. An explanation of the elastic properties will be supplied from the perspective of electronic structure origin.

5.3.1. Shear modulus

In Fig. 6(a), the shear modulus of NiCo solution, in a paramagnetic state, along the [110] and [11$\bar{2}$] directions increase with Co concentration: from the physical meaning of shear modulus, Co addition into NiCo solution corresponds to a strengthen effect on shear modulus and the ideal shear strength along [110] and [11$\bar{2}$] directions. A_Z decreases, as caused by the insensitivity of C_{12} to changing Co concentration (Fig. 3(a)). The anisotropies of NiCo solution in both the ferromagnetic, and paramagnetic states are lower than that of pure Ni in a paramagnetic state. The alloying effects on the shear modulus are presented in Fig. 6. In the γ' phase, the addition of Co, Ti, and W leads to an increased shear modulus in (Ni, Co)$_3$(Al, Ti), though some systems do not match this trend. In many systems with $L1_2$ structures, the addition of Co, Ti, and W results in a reduction in A_Z.

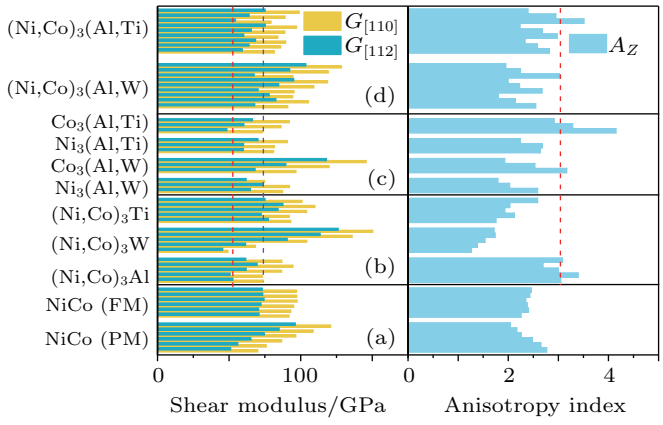


Fig. 6. (a) Directional shear modulus and the corresponding (b) anisotropy index of the systems (vertical ordinate information is consistent with that of Fig. 3).

5.3.2. Directional Young's modulus

The {110} plane includes the cubic high symmetry crystallographic directions [100], [110], and [111]. Here, we chose this cross-section to give a complete presentation of the directional Young's modulus. From the elastic constants results, we only give the Young's modulus of NiCo(PM), NiCo(FM), Co$_3$(Al, W), (Ni, Co)$_3$W, Co$_3$(Al, Ti), and (Ni, Co)$_3$(Al, W) systems. As all these systems satisfy $2S_{11} - 2S_{12} - S_{44} > 0$ in Fig. 7, the Young's modulus satisfies $E_{[100]} < E_{[110]} < E_{[111]}$, as derived from Eq. (9). The $E_{[111]}$ of $(Ni_{0.75}Co_{0.25})_3(Al_{0.25}W_{0.75})$ in Fig. 7(f) is the biggest while $E_{[100]}$ is the smallest as a result of the significant anisotropy index A_Z of 3.016 of $(Ni_{0.75}Co_{0.25})_3(Al_{0.25}W_{0.75})$ and its large elastic constants. The value of A_Z of Co$_3$W (1.710) is lower than that of Co$_3$(Al$_{0.25}$W$_{0.75}$) (1.733), corresponding to $E_{[111]}$ of Co$_3$W being lower than that of Co$_3$W(Al$_{0.25}$W$_{0.75}$) as shown in Fig. 7(c). The shape of the Young's modulus plot in Fig. 7 is closely related to the anisotropy index of these systems, as derived from Eq. (9).

5.3.3. Electronic structure

Except for the inclusion of the main crystal direction, the {110} plane also includes tetrahedral and octahedral interstices of the cubic systems. Here, we chose the {110} plane to analyze the charge density difference (Fig. 8(a)). The charge accumulates in tetrahedral interstices, which is consistent with the charge density difference of fcc Al.[57] The bonding of W atoms with its neighbors is higher than among Al atoms. The trend of bonding of Co–W is higher than that of Ni–W, especially along the [110] direction. The directional bonding character of the charge density explains why Ni$_3$W and Co$_3$W are stronger than Ni$_3$Al and Co$_3$Al. As Co and Ni are neighbors in the periodic table, the shape of their s-orbitals and p-orbitals are the same (Fig. 8(b)). Compared with a Co atom, the d-orbital of Ni moves to a deeper energy level and occupies a higher energy peak.

In the bonding as shown in Fig. 8, the s-orbital does not participate to any significant extent in bonding. For the d-orbitals, the shape and the peak position are similar, W forms a hybrid with Ni or Co below −3.35 eV. The p-orbital of W and d-orbital of Ni show p–d hybridization at around −2.2 eV, while the d-orbital of W and d-orbital of Co form a d–d hybridization at around −1.8 eV. From the bonding strength point, the Co–W bonding is stronger than that of the Ni–W bonding. However, the directionality of the Ni–W bonding is stronger than that of Co–W bonding. From Fig. 8(a), the

charge accumulation of Ni–Al and Co–Al around octahedral interstices position is similar. As the charge accumulation around Al is not obvious, the bonding of Al with its neighbours can be neglected in the (Ni, Co)$_3$(Al, W) systems, but the bonding of W with its neighbours is strong. The higher addition of Co and W allows strong directional bonding, thus corresponding to the higher elastic constants. The directionality of the bonding around Co atoms along the [011] direction is higher than that around Ni atoms. From the topology theory of the charge density,[58] this corresponds to the higher shear modulus and Young's modulus along the [011] direction. Moreover, this also causes a reduction in the anisotropy index and an increase in the G/B ratio, which means that the materials become brittle with higher Co and W additions.

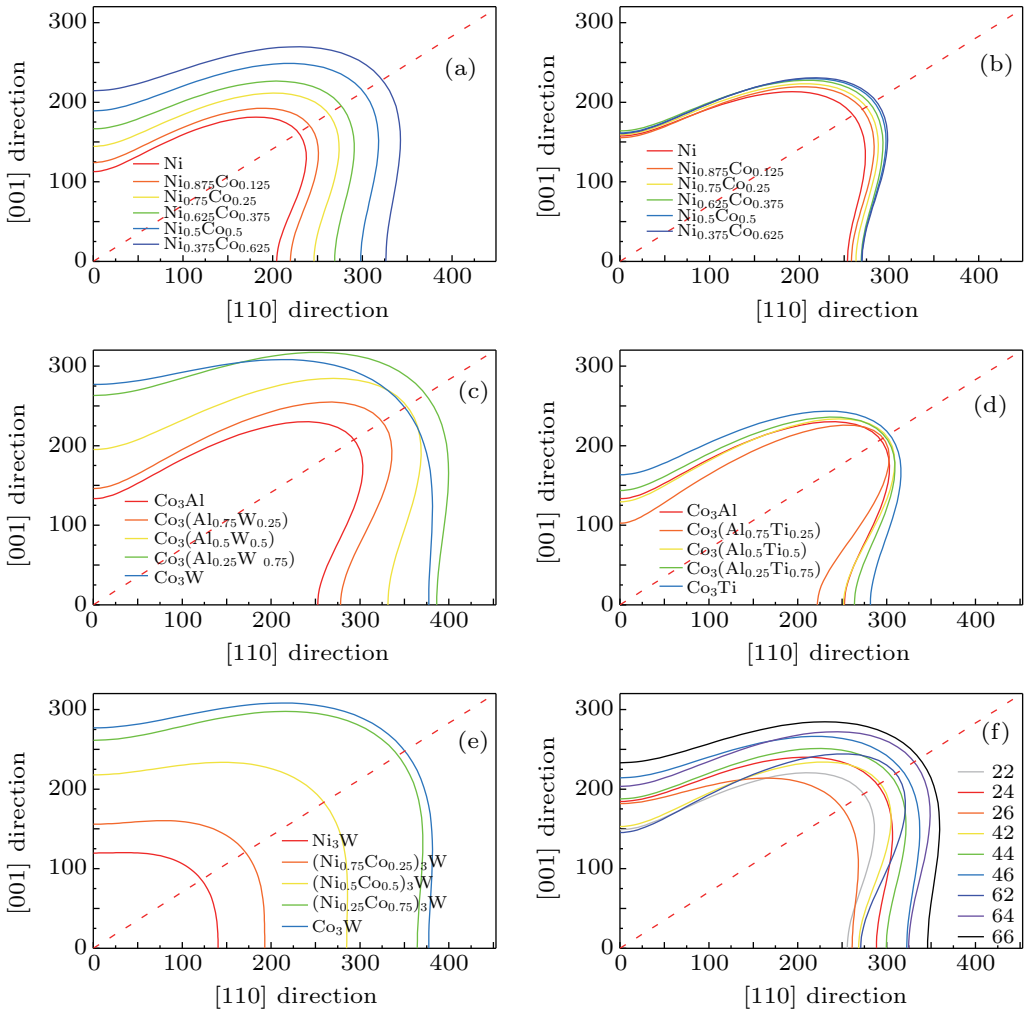


Fig. 7. Directional Young's modulus in the {110} plane for different systems: (a) NiCo systems in a paramagnetic state, (b) NiCo systems in a ferromagnetic state, (c) Co$_3$(Al, W) systems, (d) Co$_3$(Al, Ti) systems, (e) (Ni, Co)$_3$W systems, and (g) quaternary systems of (Ni, Co)$_3$(Al, W). The x direction is [110], the y direction is [001], and the red dotted line denotes the [111] direction.

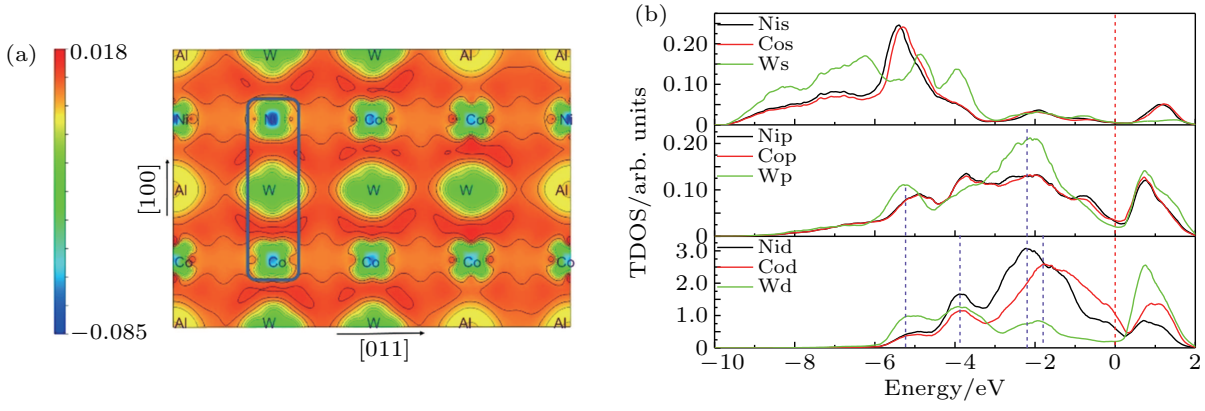


Fig. 8. The charge difference iso-surface and density of state in (Ni, Co)$_3$(Al, W) systems and the partial density of state including a W atom and its nearest neighbour Co and Ni atoms. The Ni, Co, and W in panel (b) correspond to atoms in the blue rectangle of panel (a).

6. Conclusion

The lattice constant, bulk modulus, and elastic constants of NiCo-based model systems were investigated by first principles calculation in combination with SQS. The relationship between bulk modulus and volume, stability and ductility, and elastic modulus were discussed. The key results may be summarised as follows.

(i) The lattice constants and bulk modulus of the systems vary linearly with the concentrations of Co, Ti, and W. The addition of Co, Ti, and W can regulate the lattice mismatch and bulk modulus of NiCo-based superalloys.

(ii) Co can linearly strengthen the elastic constants, shear modulus, and Young's modulus of Ni solution in a paramagnetic state, and decrease the anisotropy index simultaneously. Except for the value of C_{44} of $(Ni_{0.75}Co_{0.25})_3(Al_{0.25}W_{0.75})$, the addition of W and Ti strengthens the elastic constants of quaternary (Ni, $Co)_3$(Al, W/Ti) systems.

(iii) W exerts a strengthening effect on the elastic properties of the γ' phases, however, high W and Ni concentrations lead to instability (*e.g.*, in $(Ni_{0.75}Co_{0.25})_3(Al_{0.25}W_{0.75})$), and high W and Co concentrations result in brittle behaviour (*e.g.*, in $Co_3(Al_{0.25}W_{0.75})$).

(iv) The shear modulus and Young's modulus in a specific direction do not change monotonically with Co, Ti, and W addition. The strength and directionality of the bonding are consistent with the strengthened elastic properties and enhanced ductility of the alloys.

References

[1] Gu Y, Harada H, Cui C, Ping D, Sato A and Fujioka J 2006 *Scr. Mater.* **55** 815
[2] Gu Y F, Cui C, Ping D, Harada H, Fukuda T and Fujioka J 2009 *Mater. Sci. Eng. A-Struct. Mater. Properties Microstruct. Process.* **510–511** 250
[3] Knop M, Mulvey P, Ismail F, Radecka A, Rahman K M, Lindley T C, Shollock B A, Hardy M C, Moody M P, Martin T L, Bagot P A J and Dye D 2014 *Jom* **66** 2495
[4] Cui C Y, Gu Y F, Yuan Y, Osada T and Harada H 2011 *Mater. Sci. Eng. A-Struct. Mater. Properties Microstruct. Process.* **528** 5465
[5] Zhu J, Titus M S and Pollock T M 2014 *J. Phase Equilibria Diffus.* **35** 595
[6] Sidnov K, Belov D, Ponomareva A, Abrikosov I, Zharmukhambetova A, Skripnyak N, Barannikova S, Rogachev A, Rouvimov S and Mukasyan A 2016 *J. Alloys Compd.* **688** 534
[7] Zenk C H, Neumeier S, Engl N M, Fries S G, Dolotko O, Weiser M, Virtanen S and Göken M 2016 *Scr. Mater.* **112** 83
[8] Jones N G, Christofidou K A, Mignanelli P M, Minshull J P, Hardy M C and Stone H J 2014 *Mater. Sci. Technol.* **30** 1853
[9] Cui C Y, Gu Y F, Ping D H and Harada H 2008 *Intermetallics* **16** 910
[10] Llewelyn S C H, Christofidou K A, Araullo-Peters V J, Jones N G, Hardy M C, Marquis E A and Stone H J 2017 *Acta Mater.* **131** 296
[11] Sato J, Omori T, Oikawa K, Ohnuma I, Kainuma R and Ishida K 2006 *Science* **312** 90
[12] Zunger A, Wei S H, Ferreira L G and Bernard J E 1990 *Phys. Rev. Lett.* **65** 353
[13] Soven P 1967 *Phys. Rev.* **156** 809
[14] Sanchez J M, Ducastelle F and Gratias D 1984 *Physica A: Stat. Mech. Its Appl.* **128** 334
[15] Bellaiche L and Vanderbilt D 2000 *Phys. Rev. B* **61** 7877
[16] Wei S H, Ferreira L G, Bernard J E and Zunger A 1990 *Phys. Rev. B* **42** 9622
[17] Cowley J M 1950 *Phys. Rev.* **77** 669
[18] Vitos L 2007 *Computational quantum mechanics for materials engineers: the EMTO method and applications* (Springer Science & Business Media)
[19] Moakher M and Norris A N 2006 *J. Elasticity* **85** 215
[20] Browaeys J T and Chevrot S 2004 *Geophys. J. Int.* **159** 667
[21] von Pezold J, Dick A, Friák M and Neugebauer J 2010 *Phys. Rev. B* **81** 094203
[22] Grimvall G 1999 *Thermophysical properties of materials* (Elsevier)
[23] Nye J F 1985 *Physical properties of crystals: their representation by tensors and matrices* (Oxford University Press)
[24] Krenn C R, Roundy D, Morris J W and Cohen M L 2001 *Mater. Sci. Eng. A* **317** 44
[25] Jahnátek M, Hafner J and Krajčí M 2009 *Phys. Rev. B* **79** 224103
[26] Roundy D, Krenn C R, Cohen M L and Morris J W 1999 *Phys. Rev. Lett.* **82** 2713
[27] Voigt W 1889 *Ann. Phys.* **274** 573
[28] Reuss A 1929 *ZAMM-J. Appl. Math. Mech./Z. Angew. Math. Und Mechanik* **9** 49
[29] Hill R 1952 *Proc. Phys. Society. Sect. A* **65** 349
[30] Pugh S F 1954 *London Edinburgh Dublin Philos. Mag. J. Sci.* **45** 823
[31] van de Walle A, Asta M and Ceder G 2002 *Calphad* **26** 539
[32] van de Walle A, Tiwary P, de Jong M, Olmsted D L, Asta M, Dick A, Shin D, Wang Y, Chen L Q and Liu Z K 2013 *Calphad-Comput. Coupling Phase Diagrams Thermochemistry* **42** 13
[33] van de Walle A 2009 *Calphad-Comput. Coupling Phase Diagrams Thermochemistry* **33** 266
[34] Murnaghan F 1944 *Proc. Natl. Acad. Sci.* **30** 244
[35] Zhang W, Lin J, Xu W, Fu H and Yang G 2017 *Tsinghua Sci. Technol.* **22** 675
[36] Kresse G and Hafner J 1994 *J. Phys.: Condens. Matter* **6** 8245
[37] Kresse G and Furthmüller J 1996 *Phys. Rev. B* **54** 11169
[38] Blöchl P E 1994 *Phys. Rev. B* **50** 17953
[39] Perdew J P, Burke K and Ernzerhof M 1996 *Phys. Rev. Lett.* **77** 3865
[40] Kittel C 1996 *Introduction to Solid State Physics*
[41] Wu Q and Li S 2012 *Comput. Mater. Sci.* **53** 436
[42] Mehl M J, Klein B M and Papaconstantopoulos D 1995 *Intermetalic Compounds: Principles and Practice*, Vol. 1, pp. 195–210
[43] Yoo M H 1987 *Acta Metall.* **35** 1559
[44] Yao Q, Xing H and Sun J 2006 *Appl. Phys. Lett.* **89** 161906
[45] Jiang C 2008 *Scr. Mater.* **59** 1075
[46] Tanaka K, Ohashi T, Kishida K and Inui H 2007 *Appl. Phys. Lett.* **91** 181907
[47] Denton A R and Ashcroft N W 1991 *Phys. Rev. A* **43** 3161
[48] Nathal M 1987 *Metall. Trans. A* **18** 1961
[49] Miedema A R, Boer F R D and Chatel P F D 1973 *J. Phys. F: Met. Phys.* **3** 1558
[50] Rose J H and Shore H B 1993 *Phys. Rev. B* **48** 18254
[51] Mishra N S and Ranganathan S 1995 *Acta Metall. Mater.* **43** 2287
[52] Born M and Huang K 1954 *Dynamical theory of crystal lattices* (Clarendon Press)
[53] Gui C, Sato A, Gu Y and Harada H 2005 *Metall. Mater. Trans. A* **36** 2921
[54] Wang H, Zhang Z D, Wu R Q and Sun L Z 2013 *Acta Mater.* **61** 2919
[55] Wang F, Holec D, Odén M, Mücklich F, Abrikosov I A and Tasnádi F 2017 *Acta Materialia* **127** 124
[56] Pettifor D G 1992 *Mater. Sci. Technol.* **8** 345
[57] Nakashima P N H, Smith A E, Etheridge J and Muddle B C 2011 *Science* **331** 1583
[58] Eberhart M E 1996 *Acta Mater.* **44** 2495